A NEW LOW-PROFILE WIDE-SCAN PHASED ARRAY FOR UWB APPLICATIONS

D. Tallini *, A. Galli *, M. Ciattaglia †, L. Infante †, A. De Luca †, M. Cicolani †

* Sapienza University of Rome – Department of Electronic Engineering
Via Eudossiana 18, 00184 Roma, Italy – Fax: +39 06 4742647 – galli@die.uniroma1.it
† SELEX Sistemi Integrati S.p.A. – 'Sistemi Radianti'
Via Tiburtina, km 12,400, 00131 Roma, Italy – angdeluca@selex-si.com

Keywords: Ultra-wideband antennas, phased arrays, wide scan, microwave printed circuits, stacked patches.

Abstract

The possibility of achieving new advantageous solutions of high-performance UWB wide-scan arrays is investigated here for typical C-X band applications. Original compact, low-profile configurations of phased arrays, based on the class of the aperture-coupled stacked patches, have been analysed, designed, and tested. The relevant results show very interesting features as concerns band and scanning features.

1 Introduction

In the last years, the increasing demand in various mobile communication systems (radar, satellite, cellular applications) has pushed to continuous improvements in the research of high-performance, compact, and light-weight transmitting/ receiving elements. Printed circuits (in particular microstrip topology) are nowadays a favourite choice at microwaves for their attractive features, such as low profile, conformity, and reproducibility [1].

In many applications, the need of specialized multifunction operations (e.g., simultaneous surveillance, discrimination, tracking), the use of high data rates, and the ability to withstand adverse environmental conditions, have stimulated considerable research activity in the area of phased arrays [2]. Also, as the system integration increases, a single antenna is often required to support multiple services across ultra-wideband (UWB) frequency ranges [3,4]. The recent emergence of UWB technology has led to a number of distinct challenges. Due to usual requirement for low-power operation, the radiating elements should exhibit good impedance matching, almost linear phase response, and high radiation efficiency over the entire operating band.

Various potential applications are connected with such desirable features. For instance, in terms of achievable radar-cross-section (RCS) ranges, when a UWB antenna is used in a pulsed radar system, it can replace a large set of narrow-band radiators, as usually required to cover the spectrum of interested bands. Furthermore, in satellite communications, a single wideband feed antenna can strongly reduce space and weight when supporting many communication channels.

On this ground, the present work is aimed at investigating new advantageous solutions for high-performance UWB arrays, as concerns in particular the possibility of achieving compactness, low profile, and wide-scan ranging. Some specific design constraints in dimensions and scanning have been fixed for typical C-X band applications (4–12 GHz). Various preliminary studies have been carried out on standard and innovative topologies, in order to investigate the suitability of many types of printed configurations as single elements and then as an array. Consequently, specific novel array configurations have been tested, based on the class of antennas with aperture-coupled stacked patches [5-8].

In the following, first the analysis and the synthesis procedures of the antenna are considered (Sec. 2), then a particular finite array is completely designed and tested (Sec. 3), and some conclusions are drawn (Sec. 4).

2 Antenna element and array topologies

In the next subsections, the design methods employed are outlined (2.1), then some representative results of array performance are illustrated for both square (2.2) and triangular (2.3) lattices referring to a specific printed antenna topology.

2.1 Design approaches for the array structure

The fundamental step in this design procedure has been focused on the direct study of the overall array structure with the aim of properly evaluating, through different methods, the influence of mutual coupling on the various performance features, such as bandwidth, beam-scanning capability, and radiation-pattern stability. Due to the complexity of the usual topologies of such radiators, a commercial CAD tool (*CST Microwave Studio*™) has mainly been employed for the relevant electromagnetic analysis [9].

In order to achieve a first overall evaluation of the performance of possible array structures, the main features of the antennas have been examined through a broadband characterization at broadside, which requires limited CPU time, thus speeding up the optimization process. An infinite-array analysis has therefore been performed by referring to the 'unit cell,' making use of the 'periodic boundary conditions' (PBC) in the commercial code.

Further studies have been developed by studying the corresponding finite uniform arrays of $N \times N$ elements. Two different methods have been employed to this end: an 'ad-hoc' code, which operates a 'post-processing' of a suitable CAD implementation taking into account the coupling effects in a simplified way, and direct CAD simulations based on the 'simultaneous excitation' technique in CST. It is thus possible to compare the convergence with the infinite-array results as N varies and achieve the actual finite-array performances.

The 'post-processing procedure' is performed by evaluating, and then properly combining, the scattering parameters at the various ports when the central element is driven and all the others are properly terminated in matched loads. Thus, the 'active element pattern' can be achieved for the prediction of the scan performance in large arrays [8,10]. In fact, if all the active element factors can be assumed as equal, the pattern of the fully excited array is expressible as the product of the active element factor and the array factor, similarly to the ordinary array theory [2,10]. Thus, all the mutual coupling effects are simply accounted for, including the possibility of scan blindness, etc. On the other side, with the 'simultaneous-excitation procedure', where all the elements are driven with the same phase and amplitude, the various active element patterns and the overall array behaviour are directly achieved.

2.2 Antenna topology and array results with square lattice

In connection with the mentioned constraints (related to ultra-wideband operation, wide-scan ranging, low profile, reduced size, etc.), among the various solutions studied, a particular printed configuration has been investigated in depth, based on aperture-coupled stacked patches, which is a well-known topology to enlarge bandwidth of printed antennas [7,8].

The reference geometry of our element (unit cell) is in Fig. 1.

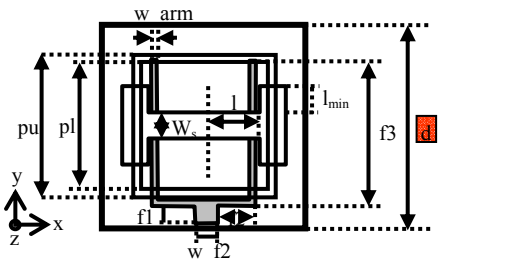

a)

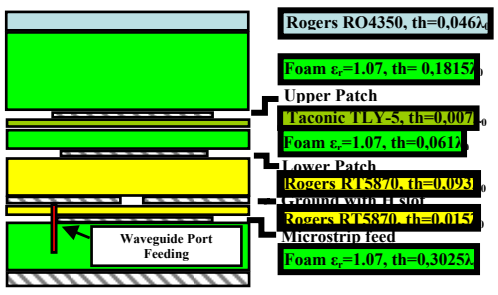

b)

Fig. 1: Geometry of our radiating element of the array (unit cell), based on aperture-coupled stacked patches: a) top view; b) lateral view.

In the top view (Fig. 1a), it is seen that a dual-offset microstrip line has been used to feed an H-shaped slot in a multilayered configuration, where a pair of stacked patches radiate. The feed line is truncated nearby the external boundary of the cell in order to place an ideal waveguide port inside the domain, as required by the CAD tool when PBC is used. The microstrip geometry has been chosen to provide a 50-Ω input impedance, as for the impedance of the coaxial line used in the transition (see also 3.1). The parameter d refers to the unit-cell size and represents the element spacing in a square lattice of the array. In the lateral view (Fig. 1b), the multilayered structure is shown, involving dielectric slabs of various materials and metal patches. At the bottom of the stack a ground plane has been placed to avoid back-radiation.

A large number of simulations has been performed on the infinite-array structure to optimize the performance of the radiating element. Several physical and geometrical parameters can be varied, sensitively affecting in particular the wide-band behaviour. Referring to the amplitude of the reflection coefficient $S_{1,1}$ (i.e, the return loss, RL), for instance, a strong influence has been observed of the width of the offset lines *w_arm* on the bandwidth (the characteristic impedance being fixed), as shown in Fig. 2. The narrowing of the offset lines provides an improvement of the band matching ($RL < -10$ dB up to 90%, for 4.2–11.6 GHz).

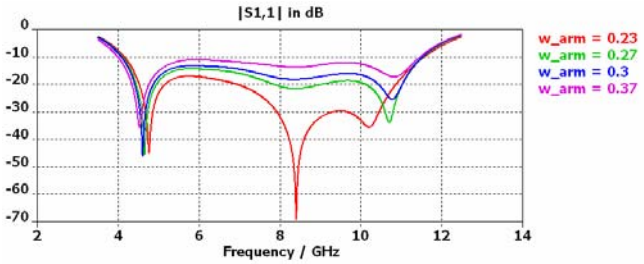

Fig. 2: Behaviour of the reflection-coefficient amplitude (return loss) as a function of frequency, for different widths of the offset lines *w_arm*, feeding the stacked structure (infinite array with the unit-cell analysis).

This infinite-array approach provides quickly basic information that also allows us to check the convergence properties of the finite array as N is increased. Several array sizes have been simulated by changing the number of elements. Some relevant results are illustrated in Fig. 3 for the active element patterns in the case of an $N = 15$ phased array with a square lattice. The behaviour of the active reflection coefficient as a function of frequency, for different values of scan angles is given in Fig. 3a for the E plane, and in Fig. 3b for the H plane. Analogous results concerning both real (R_{in}) and imaginary (X_{in}) parts of input impedance vs. frequency, for different scan angles in the E-plane case, are in Fig. 3c. All these results show a rather regular wide-band behaviour for a good range of the array scanning. As expected, by increasing the scanning, a worsening of band matching is manifest: variations of the input impedance are stronger and increasing mismatch occurs for scan angles greater than about 45°. Anyway, in this angular range, the array provides a bandwidth ($RL < -10$ dB) of almost an octave.

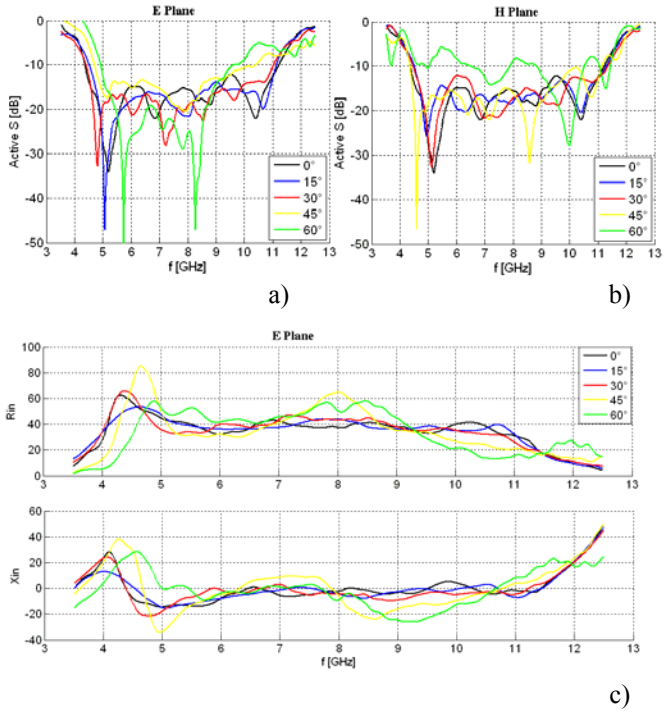

Fig. 3: Behaviour of the input parameters as a function of frequency and for different scanning angles, for an $N = 15$ square-lattice array of elements as in Fig. 1: a) Amplitude of the reflection coefficient (return loss) in the *E* plane; b) The same as in a) in the *H* plane; c) Real (*up*) and imaginary (*down*) parts of the input impedance (Ω).

The relevant radiation patterns of the $N = 15$ phased array, at various operating frequencies, have also been calculated, both in *E* and *H* planes. The results show that *H*-plane patterns are a bit larger than *E*-plane ones. The average gain is around 5 dB on both planes.

2.3 Array performance with a triangular lattice

The results shown in Fig. 3 related to beam scanning have pushed our efforts towards the use of a different arrangement in order to further improve the scanning capabilities in particular on the *E* plane, as required in our design specifics. The geometry has been changed along the proper direction, and a distribution of elements in a triangular lattice has been considered. The relevant elementary cell, shown in Fig. 4, has been designed and then optimized in this case as well.

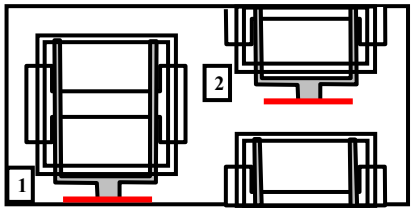

Fig. 4: Geometry of the elementary cell in a triangular lattice: two ports are included in the cell.

The application of the PBC to the triangular case is not straightforward for most commercial solvers, due to non-orthogonal boundaries in the periodicity cell, unless a large computation domain with a truncated array is considered. In the geometry of Fig. 4, examined here in the simulations, both ports included in the periodic cell are simultaneously driven with the same phase and amplitude.

In this case, the optimization process has especially been focused on the right definition of the sizes and positions for metallic components, such as the patches, the H slot, and the offset lines, paying attention to the relative location between each other which strongly affects the coupling phenomena.

Both the infinite and the $N = 15$ array cases are compared in Fig. 5, as concerns the active reflection coefficient vs. frequency at broadside ($\theta = 0°$). There is a good agreement between the two behaviours. The ripples, visible for the finite array, are connected with the truncation of the structure, which gives rise to edge effects. This element configuration provides a very good bandwidth (4.3–11.8 GHz, BW ≈ 93%).

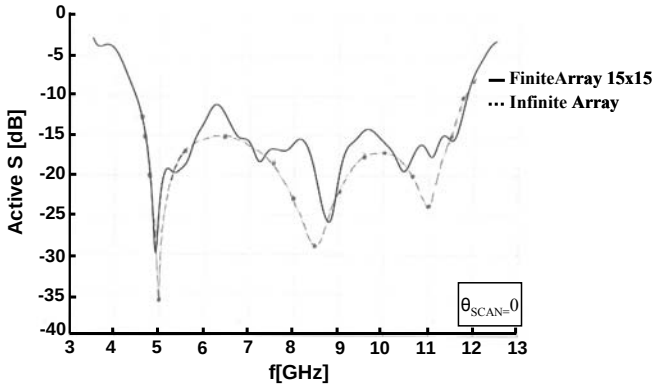

Fig. 5: Active reflection coefficient vs. frequency for the $N = 15$ array and an infinite array (triangular lattice).

In Fig. 6, active-element radiation patterns are presented at different frequencies for both planes as the elevation angle θ varies. They are quite stable over all the working band, with an average gain close to 4-5 dB. The beam-width at –3 dB is around 100° for both the principal planes.

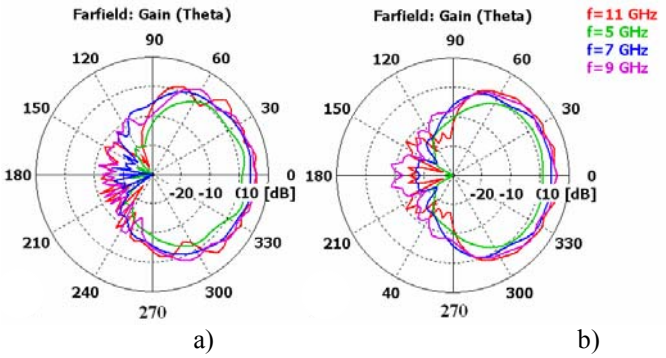

Fig. 6: Radiation patterns in polar forms of the $N = 15$ array in a triangular lattice, for different frequency values: gain as a function of θ: a) *E* plane; b) *H* plane.

By means of the data post-processing of the scattering parameters achieved with the active-element array excitation, such triangular-lattice array has shown an improved scanning capability on the *E* plane over a larger band than that obtained with the square lattice. These results are shown in Fig. 7 for *E* and *H* planes (Figs. 7a and 7b, respectively). It is seen that a larger bandwidth can be reached, i.e., about 4.5–11.5 GHz, for steering angles up to ±45° on both the principal planes.

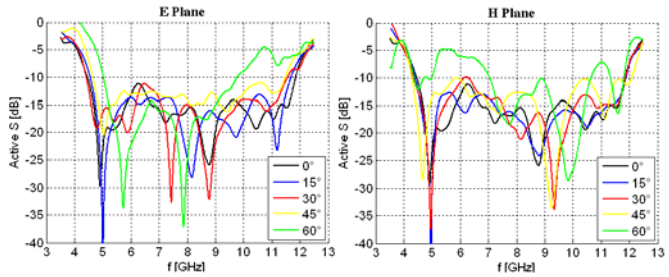

a) b)

Fig. 7: Array with an $N = 15$ triangular lattice: amplitude of the active reflection coefficient vs. frequency, for various scan angles; a) E plane; b) H plane.

Furthermore, the case with a simultaneous excitation of the array has been evaluated: the relevant results are shown in Fig. 8a for the active reflection coefficient, where different curves have been plotted, for various position of the elements in the triangular array (sketched qualitatively in Fig. 8b). It is seen that the inner elements yield a better response than the outer ones because they take advantage from mutual coupling effects. This trend is useful in the perspective of the final application, where a very large phased array with thousand of elements should be considered.

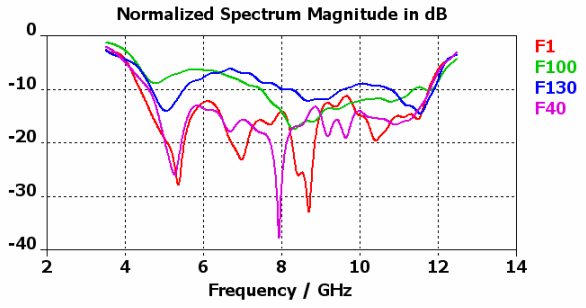

a)

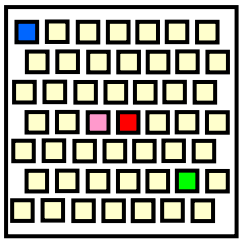

b)

Fig. 8: The 15×15 array in triangular lattice: a) reflection coefficient vs. frequency for elements sparsely chosen in the frame; b) qualitative sketch of the location of various elements in the triangular lattice.

3 Finite array configuration in practice

We present here some considerations about the practical implementation of the array, first involving the transitions in the feeding network (3.1) and then the relevant actual performance of the consequent overall structure (3.2).

3.1 Transition design

The arrangement of the feeding network, whose effects are not negligible in practice, has been another challenging issue. Taking into account the strict element spacing and the stack of the element below the H slot, a layout of a suitable coaxial/stripline/microstrip transition has been designed, as depicted in Fig. 9. An accurate study is necessary to guarantee good signal transmission with reduced losses. A truncated crown of via holes has been placed around the connection between the inner core of the coaxial and the stripline, in order to avoid undesired propagation in the substrates.

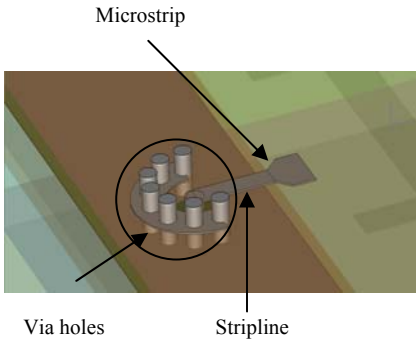

Fig. 9: A layout of the transition of the feeding lines for the array elements.

The complexity of such a structure strongly affects the simulation time. A large amount of mesh cells for the CAD analysis is necessary to achieve an accurate electromagnetic description. Good results have been obtained ($RL < -20$ dB over the entire band, with transmission losses around 0.3 dB).

3.2 Final results for the complete array

The final step of the design has been the study of the complete array structure, involving also the integration of the transitions in the elementary triangular cells. Moreover, two different aspects have been taken into account in the analysis: a solder, needed to achieve a stable ohmic connection between the inner core and the stripline, and prepreg layers with a known electric permittivity to package together the dielectric layers. At first, the infinite-array approach has been followed, as previously done, with the waveguide port at feeding. Once the performed simulations have confirmed a good behaviour, the finite array has finally been examined.

Because of the increased complexity of the more realistic cell, involving transitions etc., an array composed by 49 elements ($N = 7$) has been performed, whose analysis has required high CPU time (about 20 hs, 30 M-cells). A further outer line of dummies has been added to improve the impedance matching.

Relevant complete results of this 49-element array are presented in Fig. 10 as regards the behaviour of the reflection coefficient (Fig. 10a), the relevant radiation patterns in both planes (Fig. 10b), and the scanning performance through the reflection coefficient at different angles (Fig. 10c). It is seen in Fig. 10a the excellent ultra-wide band pattern for the reflection coefficient (more than 90% of fractional band). The results of Fig. 10b show that array provides also very stable far-field patterns in both planes, with a realized gain close to 5 dB. The scanning performances illustrated by the active reflection for different tilt angles are in agreement with the trend obtained for the previously-studied bigger array (*RL* < –10 dB for ±45° tilt on both principal planes). Obviously, a better convergence towards the infinite array is expected by increasing the array size in terms of number of elements.

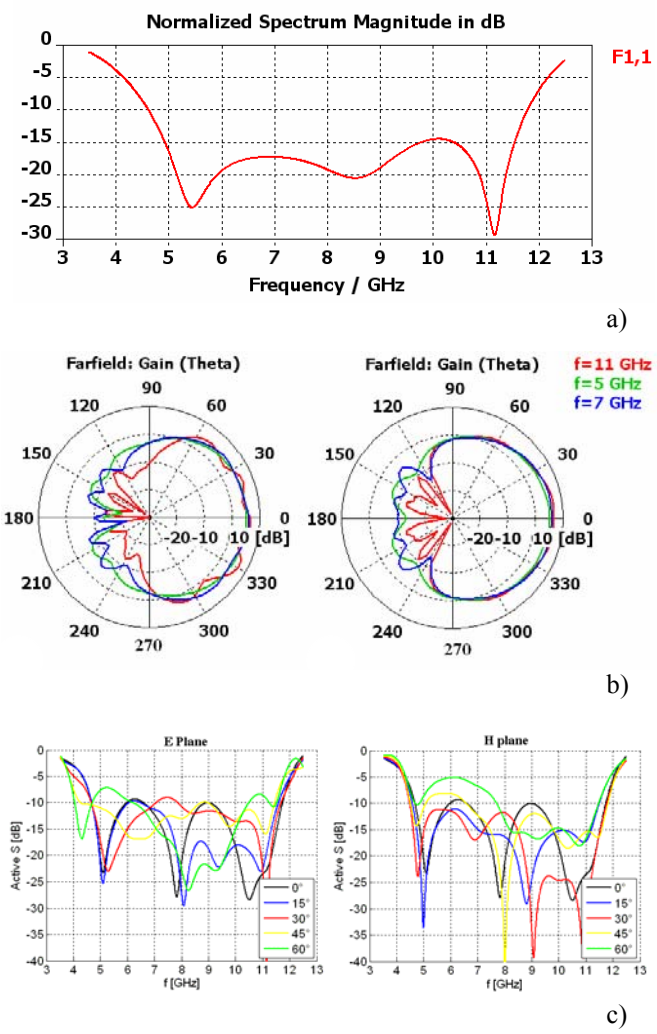

Fig. 10: Radiative features of the 49-element triangular-lattice array in the complete final implementation: a) reflection coefficient in the *E* plane vs. frequency; b) radiation patterns in polar forms for the main field component as a function of θ, for different frequency values; c) *E*-plane (*left*) and *H*-plane (*right*) reflection coefficient vs. frequency, for different scanning angles.

4 Conclusion

The aim of this investigation has been focused on the achievement of a compact, low-profile, and light-weight UWB radiating structure covering almost an octave in the C-X band with wide-scanning capabilities (at least ±45° in both the principal planes).

Based on suitable efficient design procedures to speed up the analysis and optimization processes of large phased arrays, novel UWB array configurations have been investigated, based on the class of the aperture-coupled stacked-patch antennas. As a final result, a specific implementation of a phased-array with elements arranged in a triangular lattice, has completely been designed, tested, and optimized. Attention has been paid to various technological aspects not negligible in practice, such as the arrangement of the feeding network, etc.

The proposed array has exhibited the specific requirements, in particular a large operation bandwidth (about 100%, i.e, *RL* < –10 dB inside the 4–12 GHz band), stable active element patterns and radiation diagrams in the operative frequency range, and wide-scan capabilities over the required angular tilt in both the E and the H planes.

Acknowledgments

This study has been developed in the frame of a research cooperation between "Sapienza" University and Selex SI, Rome.

References

[1] K. F. Lee, W. Chen (Eds). *Advances in microstrip and printed antennas*. Wiley, (1997).

[2] R. C. Hansen. *Phased array antennas*. Wiley, (2001).

[3] H. Schantz. *The art and science of ultra-wideband antennas*. Artech House, (2005).

[4] M. A. Peyrot-Solis, G. M. Galvan-Tejada, H. Jardon-Aguilar. "State of the art in ultra-wideband antennas", *2nd ICEEE-11th CIE Proc.*, Mexico, pp. 101-105, (2005).

[5] C. H. Tsao, Y. M. Hwang, F. Killburg, F. Dietrich. "Aperture coupled patch antenna with wide bandwidth and dual polarization capabilities", *IEEE Antennas Propagat. Soc. Symp. Dig.*, pp. 936-939, (1988).

[6] F. E. Gardiol, J. F. Zurcher. "Broadband patch antennas - A SSFIP update", *IEEE Antennas Propagat. Soc. Symp. Dig.*, pp. 2-5, (1996).

[7] S. D. Targonski, R. B. Waterhouse, D. M. Pozar. "Design of wide-band aperture-stacked patch microstrip antennas", *IEEE Trans. Antennas Propagat.*, **46**, pp. 1245-1251, (1998).

[8] R. B. Waterhouse. "Design and performance of large phased arrays of aperture stacked patches", *IEEE Trans. Antennas Propagat.*, **49**, pp. 292-297, (2001).

[9] – *CST Microwave Studio Manual*. CST, Germany, (2002).

[10] D. M. Pozar. "The active element pattern", *IEEE Trans. Antennas Propagat.*, **42**, pp. 1176-1178, (1994).